

## Nanomechanics and Raman spectroscopy of fibrillin 2 knock-out mouse bones

N. B. Kavukcuoglu · E. Arteaga-Solis ·  
S. Lee-Arteaga · F. Ramirez · A. B. Mann

Received: 21 December 2006 / Accepted: 5 June 2007 / Published online: 10 July 2007  
© Springer Science+Business Media, LLC 2007

**Abstract** Absence of fibrillin 2 (*Fbn2*), a non-collagenous bone protein, causes a connective tissue disorder called congenital contractural arachnodactyly (CCA) and has been associated with decreased bone mineral density. Nanoindentation and Raman microspectroscopy have been used to compare the mechanical and chemical properties of cortical bone from femora of *Fbn2*<sup>-/-</sup> deficient mice and their wild-type controls (*Fbn2*<sup>+/+</sup>). It was found that *Fbn2*<sup>-/-</sup> bones have significantly lower hardness and elastic modulus compared to *Fbn2*<sup>+/+</sup> bones, especially in the mid-cortical section. The Raman analysis showed little difference with genotype except for a decrease in type-B carbonate substitution in the endosteal region of *Fbn2*<sup>-/-</sup> bones. The results indicate that *Fbn2* plays a direct role in determining the mechanical properties of bone.

### Introduction

Bone is a composite tissue comprised of a mineral phase, an organic matrix and water. Bone mass in adults is maintained by coupling between bone resorption by

osteoclasts and bone formation by osteoblasts, however, when the activity levels of osteoclasts exceeds osteoblasts uncoupling takes place causing a significant loss in bone mass and increased fragility. The reduced bone mineral density (BMD) is the main cause of the most common bone disease, namely osteopenia/osteoporosis, which is characterized by the microarchitectural deterioration of bone tissue and an increase in fracture risk [1]. Both osteoblastic and osteoclastic activity are closely linked to the presence of non-collagenous bone matrix proteins. Although the organic phase of bone is 90% type I collagen, there are still considerable amounts of the non-collagenous proteins present including fibrillin 1 and 2. Investigators have proposed that the overall mix of non-collagenous proteins makes a significant contribution to the characteristic properties of bone, for instance its ability to mineralize compared to other tissues [2, 3]. It has also been reported that the non-collagenous proteins have a role in bone turnover regulation [4] and contribute to the structural integrity of bone.

Fibrillin 1 and 2 are extracellular glycoproteins that constitute the major structural components of connective tissue microfibrils. Their absence in bones can have dramatic effects on the bones' properties. The connective tissue disorders known as Marfan's syndrome and congenital contractural arachnodactyly are caused by mutations in fibrillin 1 (*Fbn1*) and fibrillin 2 (*Fbn2*), respectively [5, 6]. In addition to other manifestations, these two heritable disorders of the connective tissues have been associated with a reduction in bone mineral density [7–10]. The findings that fibrillin-rich microfibrils are widely distributed in the developing mouse and human skeleton has been interpreted to suggest key roles of these macromolecular aggregates in bone formation, growth and mineralization [11–13]. Furthermore, the fact that fibrillins are highly expressed by

---

N. B. Kavukcuoglu · A. B. Mann  
Materials Science & Engineering, Rutgers University,  
Piscataway, NJ 08854, USA

E. Arteaga-Solis · S. Lee-Arteaga · F. Ramirez  
Child Health Institute, UMDNJ-RWJMS, New Brunswick,  
NJ 08903, USA

A. B. Mann (✉)  
Biomedical Engineering, Rutgers University, Piscataway,  
NJ 08854, USA  
e-mail: abmann@rci.rutgers.edu

differentiating osteoblasts may also indicate a function in matrix adherence through interaction with the  $\alpha_v\beta_3$  integrin [11, 14, 15]. Finally, fibrillin-rich microfibrils have been associated recently with modulating the activity of TGF- $\beta$ , one of the major growth factors involved in bone physiology [16]. Consistent with these earlier lines of indirect evidence, unpublished data indicates that both fibrillin-1 and fibrillin-2 deficient mice are osteopenic due to distinct alterations in the balance of bone remodeling [17; Arteaga-Soils et al. (unpublished)].

In this study Raman spectroscopy has been used to investigate how the absence of *Fbn2* affects the chemistry of mouse bones, while nanoindentation has been used to examine the bones' mechanical properties. Raman Spectroscopy is a non-destructive way of analyzing the molecular structure of the mineral components of bone at the microscopic level. Raman can characterize both the organic and inorganic component of bone by examining the vibrational spectra of the chemical bonds. It provides quantitative information on the changes in the mineral and matrix composition as well as the nature and amounts of substituents in the mineral. These advantages of Raman Spectroscopy have led to it gaining in importance as a method to study bone [18–20] and, in particular, to examine compositional changes due to aging and diseases, and the link between bone chemistry and mechanical deformation.

Nanoindentation has become the standard tool for characterizing the mechanics of materials at small length scales because of its ability to probe a surface and map its properties with a resolution smaller than 1  $\mu\text{m}$ . Due to small dimensions of mouse bones, this technique provides an effective measurement method for their mechanical properties [21–23]. In the present study the average properties (mechanical and chemical) and the location dependent (intra-bone) variations in the properties were investigated and compared between cortical femora bones from a number of knockout (*Fbn2*<sup>-/-</sup>) and wild-type (*Fbn2*<sup>+/+</sup>) mice.

## Materials and methods

### Sample preparation

The study used 3-month old female 129/SvEv *Fbn2*<sup>-/-</sup> mouse models ( $n = 5$ ) and their age, sex and background matched wild-type controls ( $n = 6$ ). Creation of *Fbn2*<sup>-/-</sup> mice has been already described [24]. The research was approved by the Rutgers and UMDNJ-RWJMS Animal Care and Facilities Committees (Protocol # I 06–012-2) and performed according to the NIH guidelines for the care and use of laboratory animals (NIH Publication #85-23

Rev. 1985). The left femur from the mice of each genotype was used for this study. The bones were prepared for nanoindentation testing as described by Roy et al [25]. Briefly, this involved dehydration in graded alcohol solutions (70–100%) and mounting in a low temperature cure epoxy (SPI supplies, West Chester, PA). Dehydration can affect the mechanical properties of bone, however all the bones were prepared in the same way so these effects will be present in bones from both genotypes. There is a small possibility that one genotype is affected more by dehydration than the other, but this was not investigated. After mounting, the included femora were sectioned transversely at mid-shaft using a diamond wafering saw. The surfaces were ground with silicon carbide paper of decreasing grit size (400, 600 and then 1,200 particles per inch) followed by polishing with diamond paste down to 1/2 then 1/4  $\mu\text{m}$  grit size. After the polishing, all specimens were cleaned ultrasonically to remove surface debris. Raman studies do not require any specific kind of sample preparation [19], so the same bones used for nanoindentation testing were used. It should be noted that embedding samples into epoxy has been shown to have no effect on the Raman data [26]. The locations for the nanoindentation and Raman spectroscopy measurements are shown in Fig. 1.

### Raman microspectroscopy

A Renishaw inVia<sup>TM</sup> Raman microscope was used for this study with a 785 nm laser beam and a grating of 1,200 1/mm. The laser was focused on each point of interest through a Leica DMLM, 50X/0.75 NA objective providing an approximately 2  $\mu\text{m}$  spot size. All spectral acquisitions were performed in the 350–2,000  $\text{cm}^{-1}$  wavenumber range and the spots were spaced every 10  $\mu\text{m}$  in the  $x$ -(transverse) direction (see Fig. 1). Depending on the thickness of the cortex 15–20 measurements were taken. Test locations were marked by microindents prior to testing. Signal-to-noise ratio and fluorescence background were minimized by employing 18 s of exposure time and 3 times of accumulation (three separate spectra) at each measurement location.

The Wire 2 software provided by Renishaw was used to remove the background using cubic spline interpolation at each acquisition. A single spectrum for each sample point was obtained by averaging the three accumulations. The software was then used to analyze the peaks after Gaussian–Lorentzian curve fitting. The intensities of the following peaks were measured: phosphate  $\nu_1$  at  $\sim 958 \text{ cm}^{-1}$  ( $\text{PO}_4^{3-}$  symmetric stretching band), carbonate  $\nu_1$  at  $\sim 1,071 \text{ cm}^{-1}$  ( $\text{CO}_3^{2-}$  symmetric stretching band),  $\text{CH}_2$  wag at  $\sim 1,450 \text{ cm}^{-1}$  (C–H bending band), amide  $\sim 1,667 \text{ cm}^{-1}$  (C=O stretching band), amide III at  $\sim 1,243 \text{ cm}^{-1}$  (in-phase combination of the N–H bending and C–N stretching) and the width (full width at half maximum, FWHM) of phosphate  $\nu_1$  at around

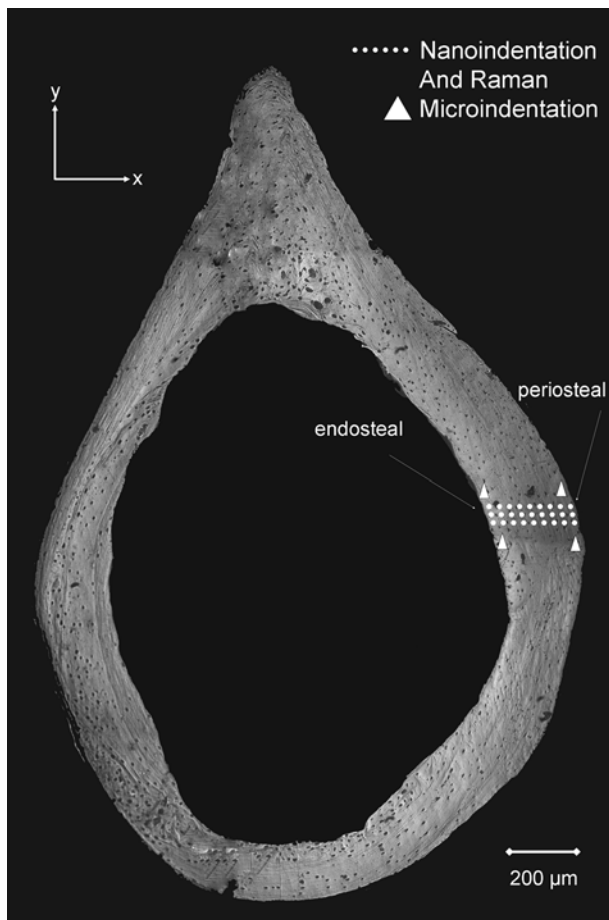


**Fig. 1** Optical image (Leica, 5 $\times$ ) looking down on a mouse femur's transverse section. Microindentations were performed to mark the test areas. The white marks represent the grid pattern of nanoindentations. Raman tests were performed on the same area as the nanoindentation, but the Raman was between the lines of nanoindentations to avoid any possibility of the two testing methods affecting each other. All tests were started at the periosteal and ended at the endosteal regions of bone

958  $\text{cm}^{-1}$ . A typical Raman spectrum for cortical mouse bone is shown in Fig. 2.

The degree of mineral to organic ratio for each sample was calculated by taking the ratio of the intensities of the  $\text{PO}_4^{3-} \nu_1$ /amide I peaks [27]. An increase in this ratio typically indicates a more mineralized matrix [18, 20], though a change in the proteins could also affect the peak ratio. In bone, two types of carbonate substitutions have been reported. Type-A carbonate substitution is when the  $\text{CO}_3^{2-}$  ion substitutes for the  $\text{OH}^-$  ion, and type-B carbonate substitution is when the  $\text{CO}_3^{2-}$  ion substitutes for the  $\text{PO}_4^{3-}$  ion [18, 28–30]. In the present study the type-B carbonate substitution was quantified by the ratio of the peak intensities for  $\text{CO}_3^{2-}$  ( $\sim 1,071 \text{ cm}^{-1}$ )/ $\text{PO}_4^{3-} \nu_1$  ( $\sim 958 \text{ cm}^{-1}$ ). Type-A substitution, however, could not be quantified because the wavenumber for the vibrational signal for this substitution ( $\sim 1,108 \text{ cm}^{-1}$ ) was very weak and could not be

observed with the Raman system. In addition, the bandwidth (FWHM) of the  $\text{PO}_4^{3-} \nu_1$  ( $\sim 958 \text{ cm}^{-1}$ ) peak was calculated to assess the crystallinity of each sample. It has been reported by a number of researchers that as the mineral crystallinity improves the bandwidth of the  $\text{PO}_4^{3-} \nu_1$  peak decreases [29, 31]. Mineral crystallinity in this case refers to an increase in the crystal size and/or atomic ordering.

### Nanoindentation

In this study, the nanoindentation tests were performed using a Triboindenter<sup>TM</sup> (Hysitron Inc., MN) in load control mode. All samples were tested in the ambient environment. Prior to testing the bones, the contact area,  $A_c$ , was determined by analysis of the load-depth curve and calibrating the tip on a standard material (fused quartz) as described by Oliver and Pharr [32]. The tip was nominally a diamond Berkovich pyramid and the loading direction was parallel to the long axis of the femur. For each indent a maximum load of 1,000  $\mu\text{N}$  was applied with a 2 s hold time at peak load. A grid pattern of  $3 \times 100$  ( $\sim 300$  indents) was performed across the cortical transverse sections of each bone (Fig. 1).

The test area was marked by microindents for each specimen. Nanoindentation tests were performed after the Raman and the location of the indentation arrays were chosen to be at approximately the same location as the Raman spectral measurements to allow a comparison between the mechanical and chemical data for each sample. Nanoindents were spaced every 2.5  $\mu\text{m}$  and 10  $\mu\text{m}$  in the  $x$ -(transverse) and  $y$ -(tangential) directions, respectively (the minimum spacing was at least 10 times the maximum nanoindent depth). The Oliver and Pharr method [32] was used to determine the mechanical properties. This method uses the following equations to find the bone's elastic modulus,  $E_s$ , and hardness,  $H$ :

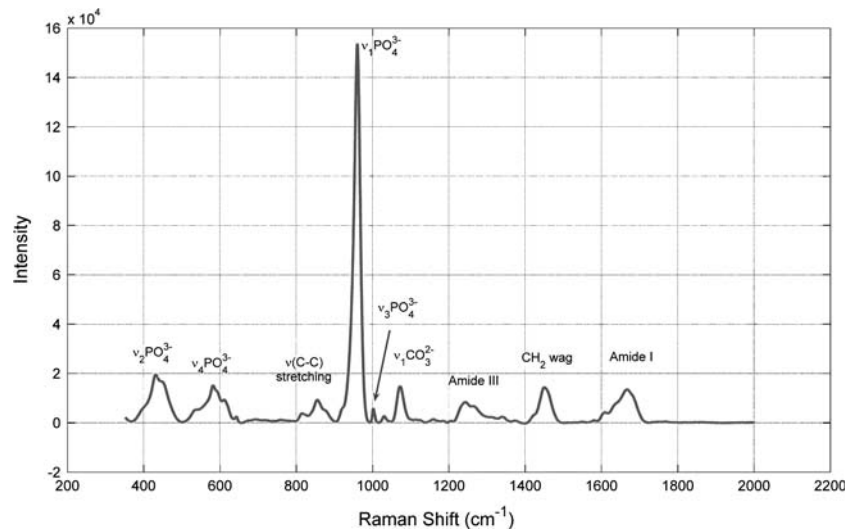
$$E_r = \frac{\sqrt{\pi} S}{2 \sqrt{A_c}}, \quad E_r = \left[ \frac{1 - \nu_s^2}{E_s} + \frac{1 - \nu_i^2}{E_i} \right]^{-1}, \quad H = \frac{P_{\max}}{A_c}$$

where,  $E_r$  is the reduced elastic modulus,  $S$  is the measured contact stiffness,  $P_{\max}$  is the maximum load and  $A_c$  is the contact area.  $\nu_i$  and  $\nu_s$  are Poisson's ratio for the indenter and sample, respectively. The values for the diamond indenter tip are  $E_i = 1,140 \text{ GPa}$ ,  $\nu_i = 0.07$  and the Poisson's ratio for the bone was taken to be  $\nu_s = 0.3$ .

### Statistical analysis

For each sample the Raman and nanoindentation data were average so a single value for each property, such as hardness, was obtained. These values were then averaged for all of the samples of each genotype to give the mean

**Fig. 2** Typical Raman spectrum of cortical bone from a mouse femur



value of the property for the genotype. ANOVA was then used to examine the statistical significance of differences between the genotypes.

The Raman spectra and the nanoindentation across the transverse axis of each knock-out and wild-type bone were examined to give the intra-bone variations for each genotype. Mechanical and chemical properties were calculated at each measurement location for each individual sample. The nanoindentation data collected across the cortical thicknesses of each bone were then divided into seven equal sections. Sections I and II are the bone adjacent to periosteal (outer) surface. Sections III–V are the mid-cortical and sections VI–VII are the bone adjacent to the endosteal (inner) surface (Fig. 1). For the Raman spectral measurements because of the larger spot size of the micro-Raman compared to the nanoindent size and the lower number of measurements (15–20) across the cortical thickness it was divided into three equal sections (I—periosteal, II—mid-cortical and III—endosteal). The mechanical and chemical properties were averaged over each section for each specimen. The mean values of the properties for each section were then averaged over all the bones of each genotype. ANOVA was conducted to assess the significance of the differences between the knock-out and wild-type mouse bones in each transverse section. All tests used 95% minimum level of confidence and  $p \leq 0.05$  was considered statistically significant.

**Results**

**Nanoindentation**

First, the mean values of  $H$  and  $E$  across the entire section of cortical bone, plus the standard deviations and the standard errors for both genotypes ( $Fbn2^{-/-}$  and  $Fbn2^{+/+}$ ) were calculated (see Table 1). ANOVA revealed that bones from  $Fbn2^{-/-}$  mice exhibited significantly lower hardness and elastic modulus values compared to bones from  $Fbn2^{+/+}$  mice ( $p < 0.05$ ). The average  $H$  and  $E$  of  $Fbn2^{-/-}$  mouse bones were  $1.15 \pm 0.01$  GPa and  $29.3 \pm 0.3$  GPa, respectively. For  $Fbn2^{+/+}$ ,  $H$  was  $1.23 \pm 0.01$  GPa and  $E$  was  $31.8 \pm 0.3$  GPa.

The intra-bone variations were plotted as bar charts to show the variation of  $H$  and  $E$  with genotype across the transverse axis of the cortical bone (Fig. 3). Individual specimens from the same genotype exhibited similar variations with respect to location. The results show that  $Fbn2^{-/-}$  mice bones have lower  $H$  and  $E$  at locations II–VII compared to the  $Fbn2^{+/+}$  mice bones. This difference between the genotypes was statistically significant ( $p < 0.05$ ) in the mid-cortical region, sections III–V. The  $H$  and  $E$  values of bones from  $Fbn2^{-/-}$  mice both decreased between the periosteal (sections I and II) and mid-cortical (sections III–V), then increased slightly towards the endosteal (sections VI and VII) part of the bone’s cross-section.

**Table 1** Average bone parameters and standard errors derived from nanoindentation and Raman spectra of bones from  $Fbn2^{-/-}$  mice and  $Fbn2^{+/+}$  mice

| Genotype     | Hardness, $H$ (GPa) | Elastic modulus, $E$ (GPa) | Mineral: organic $PO_4^{3-}$ $v_1$ /amide I | Carbonate substitution $CO_3^{2-}/PO_4^{3-}$ $v_1$ | Crystallinity $1/PO_4^{3-}$ $v_1$ (FWHM) |
|--------------|---------------------|----------------------------|---|--|--|
| $Fbn2^{-/-}$ | $1.15 \pm 0.01$     | $29.3 \pm 0.3$             | $15.02 \pm 0.2$                             | $0.110 \pm 0.0005$                                 | $0.0530 \pm 0.0002$                      |
| $Fbn2^{+/+}$ | $1.23 \pm 0.01$     | $31.8 \pm 0.3$             | $14.63 \pm 0.3$                             | $0.115 \pm 0.0023$                                 | $0.0529 \pm 0.0002$                      |

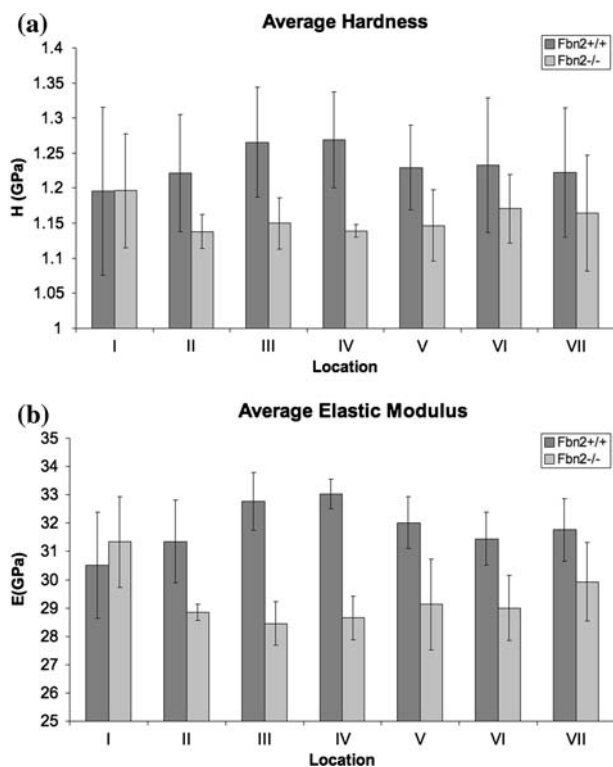


**Fig. 3** Intra-bone variations in (a) hardness,  $H$ , and (b) elastic modulus,  $E$ , for femoral cortical bones from  $Fbn2^{-/-}$  and  $Fbn2^{+/+}$  mice. Sections I and II are the bone adjacent to periosteal surface. Sections III–V are the mid-cortical and sections VI–VII are the bone adjacent to the endosteal surface. The data were taken along a grid traverse between the outer periosteal and inner endosteal regions of bone as shown by Fig. 1.  $Fbn2^{-/-}$  and  $Fbn2^{+/+}$  bones exhibit statistically significant differences in mechanical properties between sections III and V ( $p < 0.05$ ). All other differences were of low statistical significance. The error bars are standard statistical errors

For the bones from  $Fbn2^{+/+}$  mice, the variation in the  $H$  and  $E$  values followed an opposite trend where the values increased from the periosteal (sections I and II) to mid-cortical (sections III–V), but decrease near the endosteal (sections VI and VII). Note that the individual bone samples of each genotype showed similar variations with location to those seen in the average mechanical properties.

#### Raman analysis

The Raman spectra for the cortical bone specimens from both genotypes were analyzed across the entire bone and also for the three transverse sections. The mean values (across the entire cross-section of the cortical bone) and the standard errors of the phosphate  $\nu_1$ /amide I ratio, type-B carbonate/amide I ratio, and  $1/\text{Phosphate}_{(\text{FWHM})}$  are given for each genotype in Table 1. The results show the mineral:organic ratio and crystallinity were increased, and type-B carbonate substitution were decreased in  $Fbn2^{-/-}$  mouse bones, but these results had low statistical significance

when considering the average over the entire cross-section of the bone.

Intra-bone variations of the bone parameters were plotted across the transverse axis of the cortical mouse femora bones as shown in Fig. 4. Bones from  $Fbn2^{-/-}$  mice exhibited a similar mineral: organic ratio to bones from  $Fbn2^{+/+}$  mice at the periosteal and mid-cortical regions (I and II), but the mineral: organic ratio for  $Fbn2^{-/-}$  bones was higher (though not statistically significant) in the near

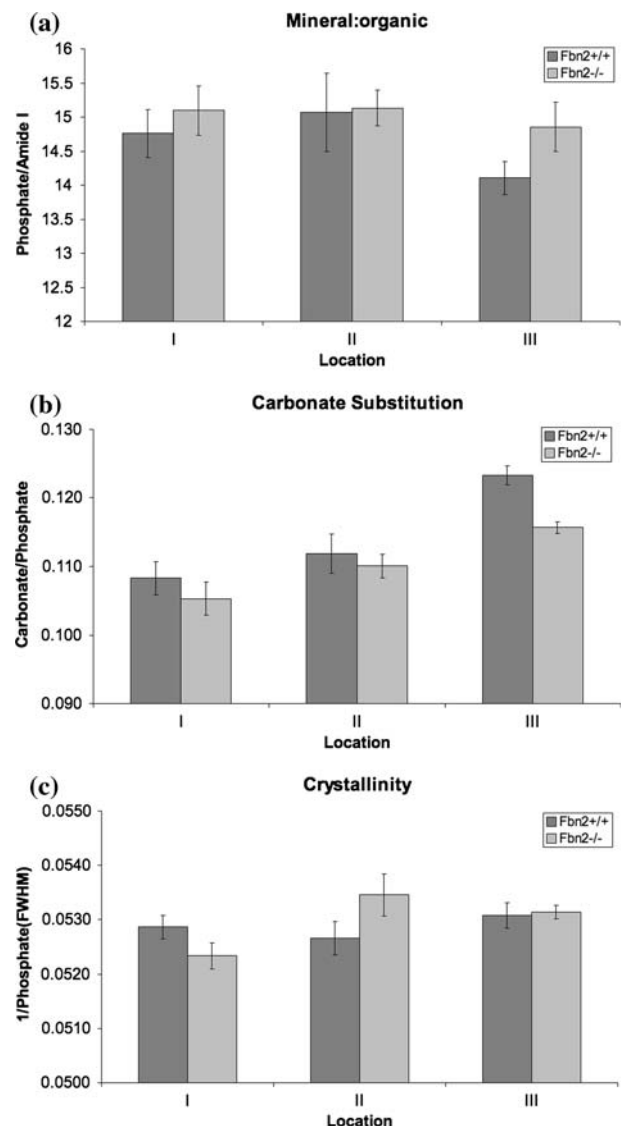


**Fig. 4** Intra-bone variations in (a) mineral:organic ratio, (b) type-B carbonate substitution and (c) crystallinity for femoral cortical bones from  $Fbn2^{-/-}$  and  $Fbn2^{+/+}$  mice. Section I is the bone adjacent to periosteal surface. Section II is mid-cortical and section III is the bone adjacent to the endosteal surface. The data were taken along a line traverse between the outer periosteal and inner endosteal regions of the bone. Type-B carbonate substitution of  $Fbn2^{-/-}$  and  $Fbn2^{+/+}$  bones exhibit a statistically significant difference in section III ( $p < 0.05$ ). All other differences were of low statistical significance. The error bars are standard statistical errors

endosteal region (III) (Fig. 4a). Type-B carbonate substitution was significantly lower in *Fbn2*<sup>-/-</sup> mouse bones at the near endosteal region compared to *Fbn2*<sup>+/+</sup> mouse bones ( $p < 0.05$ ), as seen in Fig. 4b. The crystallinity exhibited the greatest difference in the mid-cortical where it was higher for *Fbn2*<sup>-/-</sup> mouse bones compared to *Fbn2*<sup>+/+</sup> mouse bones (see region II on Fig. 4c), though this was of low statistical significance.

Overall the Raman data showed only minor differences between the apatite phase of the bones from the two genotypes. The only difference that was of statistical significance was for carbonate substitution in the endosteal region.

## Discussion

This study has investigated the role of fibrillin 2 (*Fbn2*), on the mechanical and chemical properties of cortical bone from mouse femora. Specifically, the average and location dependent differences between *Fbn2*<sup>-/-</sup> and *Fbn2*<sup>+/+</sup> mice bones have been investigated.

*Fbn2* deficiency caused a statistically significant decline in the average mechanical properties as measured by nano-indentation of mouse bones from sex and age matched knock-out and wild-type genotypes. Further to this, the location dependent analyses revealed that the difference is predominantly in the mid-cortical sections where the bones from *Fbn2*<sup>-/-</sup> mice exhibited significantly lower *H* and *E* compared to the *Fbn2*<sup>+/+</sup> mouse bones. The endosteal and periosteal showed no statistically significant difference in mechanical properties with genotype. The sections of bone showing the most significant changes in mechanical properties with genotype correspond to the sections showing differences in crystallinity, though the crystallinity differences were of low statistical significance (possibly due to the size of the sample set). The effects of genotype on mechanical properties were mostly confined to the mid-cortical section which comprises the mature bone, while the differences in mechanical properties with genotype in the periosteal and endosteal regions were much smaller. This suggests that mature lamellar bone has properties which show a different dependence on *Fbn2* than immature woven bone. Specifically, it appears that the absence of *Fbn2* reduces the mechanical properties in the fully mineralized matrix. This finding is consistent with a previous suggestion based solely on a gene expression data of a structural role for microfibrils in the mature bone [11, 13, 33]. It also agrees with unpublished data indicating an increase in bone fragility in *Fbn2*<sup>-/-</sup> mice (Arteaga-Soils et al. (unpublished)).

Another interesting finding of this study was the decreased type-B carbonate substitution in *Fbn2*<sup>-/-</sup> mouse bones. This was mostly seen in the endosteal region where

the type-B carbonate substitution of *Fbn2*<sup>-/-</sup> was significantly lower than that of *Fbn2*<sup>+/+</sup> bones.

Overall the observed effects of *Fbn2* deficiency on the mechanical properties of mouse bones indicate that the protein plays a direct role in determining the mechanics of the bones. The Raman data shows that the difference with genotype in the apatite phase of the bone matrix is not of statistical significance except for a decrease in carbonate substitution in the absence of *Fbn2* in the endosteal region. All the other differences in the Raman data were of low statistical significance. Based on this it seems unlikely that the differences in mechanical properties due to the absence of *Fbn2* were due to changes in the apatite phase.

## Conclusions

This study has demonstrated that at the nano-scale *Fbn2*, a non-collagenous bone protein, is critical in determining the mechanical properties and, to a much lesser extent, the chemical properties of bones. In bones from *Fbn2*<sup>+/+</sup> mice, hardness and elastic modulus were higher, especially in the mid-cortical region compared to bones from *Fbn2*<sup>-/-</sup> mice. Typically the mechanical properties of bone would be expected to increase with increasing crystallinity, but this is not seen in these results as crystallinity appeared to be higher in the mid-cortical region of the *Fbn2*<sup>-/-</sup> bones, though this was of low statistical significance. This suggests that the fibrillin (microfibrils) in the wildtype mouse bones may be contributing directly to its mechanical properties. The decreased mechanical properties did to a limited extent correspond to a decrease in carbonate substitution in the apatite phase. However, the most significant decrease in carbonate substitution was observed only in the endosteal region where the mechanical properties did not show a statistically significant difference with genotype.

In summary, the mechanical properties of mouse cortical bone show a clear dependence on the presence of fibrillin 2. This is most noticeable in the mature mid-cortical bone and it does not appear to be due to changes in the bone's mineral (apatite) phase. Thus, it is concluded that fibrillin 2 and, consequently, microfibrils play a direct role in determining the mechanical properties of bone.

**Acknowledgments** The authors would like to thank Prof. David Denhardt of Rutgers University, NJ and Prof. Nejat Guzelsu of UMDNJ, NJ for helpful discussions. Financial support for this research has been provided by NSF, ACS PRF, DOD DURIP, NJCHE, NIH and the Rutgers University Busch Bequest.

## References

1. Ammann P (2003) Therapie 58:403
2. Gundberg CM (2003) Osteoporosis Int 14:S37

3. Roach HI (1994) *Cell Biol Int* 18:617
4. Kaartinen MT, Pirhonen A, LinnalaKankkunen A, Maenpaa PH (1997) *J Biol Chem* 272:22736
5. Putnam EA, Zhang H, Ramirez F, Milewicz DM (1995) *Nat Genet* 11:456
6. Quondamatteo F, Reinhardt DP, Charbonneau NL, Pophal G, Sakai LY, Herken R (2002) *Matrix Biol* 21:637
7. Carter N, Duncan E, Wordsworth P (2000) *Rheumatology* 39:307
8. Dallas SL, Keene DR, Bruder SP, Saharinen J, Sakai LY, Mundy GR, Bonewald LF (2000) *J Bone Mineral Res* 15:68
9. Giampietro PF, Peterson M, Schneider R, Davis JG, Raggio C, Myers E, Burke SW, Boachie-Adjei O, Mueller CM (2003) *Osteoporosis Int* 14:559
10. Kohlmeier L, Gasner C, Bachrach LK, Marcus R (1995) *J Bone Mineral Res* 10:1550
11. Zhang H, Hu W, Ramirez F (1995) *J Cell Biol* 129:1165
12. Plantin P, Durigon M, Boileau C, Le Parc JM (2000) *Annales De Pathologie* 20:115
13. Keene DR, Sakai LY, Burgeson RE (1991) *J Histochem Cytochem* 39:59
14. Ramirez F, Pereira L (1999) *Int J Biochem Cell Biol* 31:255
15. Sakamoto H, Broekelmann T, Cheresh DA, Ramirez F, Rosenbloom J, Mecham RP (1996) *J Biol Chem* 271:4916
16. Neptune ER, Frischmeyer PA, Arking DE, Myers L, Bunton TE, Gayraud B, Ramirez F, Sakai LY, Dietz HC (2003) *Nature Genet* 33:407
17. Jones KB, Sponseller PD, Erkula G, Sakai L, Ramirez F, Dietz HC, Kost-Byerly S, Bridwell KH, Sandell L (2006) Symposium on the musculoskeletal aspects of marfan syndrome: meeting report and state of the science, p n/a
18. Akkus O, Adar F, Schaffler MB (2004) *Bone* 34:443
19. Morris MD, Finney WF (2004) *Spectrosc Int J* 18:155
20. McCreadie BR, Morris MD, Chen T-C, SudhakerRao D, Finney WF, Widjaja E, Goldstein SA (2006) *Bone* 39:1190
21. Akhter MP, Fan Z, Rho JY (2004) *Calcified Tissue Int* 75:416
22. Chen Q, Rho JY, Fan Z, Lauderkind SJF, Raghov R (2003) *Calcified Tissue Int* 73:387
23. Silva MJ, Brodt MD, Fan Z, Rho J-Y (2004) *J Biomech* 37:1639
24. Arteaga-Solis E, Gayraud B, Lee SY, Shum L, Sakai L, Ramirez F (2001) *J Cell Biol* 154:275
25. Roy ME, Rho JY, Tsui TY, Evans ND, Pharr GM (1999) *J Biomed Mater Res* 44:191
26. Carden A, Morris MD (2000) *J Biomed Optics* 5:259
27. Boskey A, Mendelsohn R (2005) *J Biomed Optics* 10(3):031102
28. Freeman JJ, Wopenka B, Silva MJ, Pasteris JD (2001) *Calcified Tissue Int* 68:156
29. Penel G, Leroy G, Rey C, Bres E (1998) *Calcified Tissue Int* 63:475
30. Yerramshetty JS, Lind C, Akkus O (2006) *Bone* 39:1236
31. Akkus O, Polyakova-Akkus A, Adar F, Schaffler MB (2003) *J Bone Mineral Res* 18:1012
32. Oliver WC, Pharr GM (1992) *J Mater Res* 7:1564
33. Kitahama S, Gibson MA, Hatzinikolas G, Hay S, Kuliwaba JL, Evdokiou A, Atkins GJ, Findlay DM (2000) *Bone* 27:61